21 July 1972, Volume 177, Number 4045 SCIENCE

Orbiting Astronomical Observatory: Review of Scientific Results

Arthur D. Code and Blair D. Savage

The second orbiting astronomical observatory (OAO-2) has been successfully carrying out astronomical investigations in the ultraviolet since launch on 7 December 1968 (*1*). Operating above the ultraviolet-absorbing layers of the earth's atmosphere, the OAO spacecraft is capable of pointing telescopes to approximately 1 minute of arc in the direction of any selected celestial object and maintaining that pointing direction to approximately 1 second of arc. In addition, the spacecraft has command and data links with the ground control stations. It is in every sense a versatile astronomical space observatory.

The observatory contains instrument packages from the University of Wisconsin and from the Smithsonian Astrophysical Observatory. In this article, we present data obtained with the photometric instruments of the University of Wisconsin, and we are primarily concerned with data analysis by astronomers from this university (*2*). The Wisconsin equipment consists of five telescopes employing photoelectric filter photometers over the spectral region from approximately 1200 to 4000 angstroms (Å), and two objective-grating scanning spectrophotometers. The spectrophotometers provide spectral resolutions of about 10 Å in the region from 1100 to 2000 Å and about 20 Å in the region from 2000 to 4000 Å. The photometric accuracy and long-term stability of most of these instruments has been exceptionally good. Details of instrumental operation and reliability can be found in Code *et al.* (*3*).

One of the major objectives of OAO-2 is to determine the spectral energy distributions of stars in the ultraviolet. Ultraviolet magnitudes for a large number of stars of diverse types are provided by the OAO filter photometers. Such information yields the basic data for determinations of stellar effective temperatures, bolometric corrections, chemical compositions, and interstellar extinctions. This information will ultimately be provided in the form of a catalog of ultraviolet magnitudes.

Figure 1 shows some stellar intensity data in the form of a color-color diagram in which the difference between the magnitude at 1700 Å and the visual (V) magnitude is plotted against the difference between the blue (B) and visual photoelectric magnitudes. The stars represented in Fig. 1 are not heavily reddened by interstellar extinction. Note the very large range of ultraviolet magnitudes for stars of different types. The $(1700 - V)_0$ color changes approximately ten magnitudes for every one-magnitude change in $(B-V)_0$ color. Since the photometric accuracy of the OAO-2 ultraviolet measurements is comparable to that of the $B-V$ determinations, the ultraviolet color provides a much more sensitive measurement of the differences among stars. There are no large systematic effects due to luminosity classes or to rotation among the stars in Fig. 1. If metallic-line stars were included they would fall below the relation exhibited here for "normal" stars. The observed color-color diagram is in excellent agreement with predictions based on the best recent theoretical model atmospheres.

For brighter stars, more detailed information on spectral energy distributions is provided by the scanning spectrometers. Figure 2 shows the spectrum of the star δ Scorpii in the region 1050 to 1500 Å. This spectrum was obtained by combining digital counts from four independent scans, each made with the normal stepping interval of 10 Å between data points but displaced 2.5 Å for each successive scan. The agreement among these independent scans is typical of the repeatability and stability of this spectrometer, which has shown no significant degradation over a 3-year period. A number of ultraviolet absorption lines are indicated in Fig. 2. The strongest absorption lines in this spectral region for early-type stars are the Lyman-alpha line at 1216 Å and the resonance lines of Si IV and C IV at 1400 and 1550 Å, respectively. The Lyman-alpha line in δ Scorpii is primarily due to interstellar atomic hydrogen (H I). The apparent drop in flux in Fig. 2 toward the shorter wavelengths is due to the decreasing scanner sensitivity. The correct stellar energy distribution can be recovered by dividing the digital counts by the known instrumental sensitivity function determined from preflight calibrations and recent, calibrated measurements of selected stars from rockets. Spectral energy distributions based on spectrometer measurements are being derived for approximately 150 stars to supplement the filter photometry data. The photometers used in the rocket calibration flights were calibrated with ultraviolet synchrotron radiation from a laboratory source and should enable us to provide ultraviolet energy distributions with an accuracy of about 10 percent.

In the following sections we describe

Dr. Code is professor of astronomy and Dr. Savage is assistant professor of astronomy at the University of Wisconsin, Madison 53706.

results of some of the investigations currently being carried out with OAO data and indicate the types of investigation that can be conducted with this first stellar space observatory. The subjects range from solar system objects to extragalactic systems.

Ultraviolet Observations of Comets

The first observations of a comet in the vacuum ultraviolet occurred on 14 January 1970, when OAO-2 recorded the ultraviolet spectrum of Comet Tago-Sato-Kosaka (1969g) (*4*). Spectrophotometric measurements of this comet were continued throughout January of that year. The observations revealed, among other things, the extensive Lyman-alpha hydrogen halo first predicted by Biermann and Trefftz (*5*). On 28 January astronomers from Princeton University obtained a photograph of the comet's nucleus in Lyman alpha that revealed its finer-scale structures (*6*). In February 1970 the bright Comet Bennett (1969i) became observable. On the basis of the OAO discovery, the orbiting geophysical observatory OGO-V made several measurements of the comet with instruments with low spatial resolution, which were capable of following the hydrogen halo out to fainter isophotes (*7*). However, OAO-2 was able to continue systematic observations both at Lyman alpha and in other spectral regions to follow the temporal changes in the comet's brightness.

A variety of circumstantial arguments suggested that water ice was the most abundant cometary ice and that the evaporation of water could account for the comets' comas. The subsequent photodissociation of water should yield primarily atomic hydrogen and OH radicals with smaller amounts of molecular hydrogen and neutral atomic oxygen (O I). However, until the OAO observations, only OH among these products had been detected and, because of the strong atmospheric absorption at 3090 Å and the low f-number, accurate intensities, isophotes, and variations with solar distance of the OH emission were not known. The OAO measurements provide data on the distribution and temporal variations of OH, H, and O I and establish an upper limit to the H_2 abundance.

Figure 3 shows OAO-2 spectral scans of Comet Bennett. Features due to H I and O I and to OH, NH, and CN radicals are identified in this spectrum. Since the OAO scanners are objective-grating spectrometers the line profiles are related to the spatial distribution of the emissions. One minute of arc corresponds to 10 Å. The full width at half intensity of the Lyman-alpha emission line corresponds to an angular size of 13 minutes for the hydrogen halo. This is about half the angular diameter of the sun. The great abundance of OH is indicated in Fig. 3 by the greater intensity of the OH band at 3090 Å than of the strong CN band at 3883 Å. The OH emission is about three times as strong as the CN emission, although the solar spectrum is three times as intense in the region of the CN band and the f-number for CN is about 24 times as great. Thus, OH is more than 200 times as abundant as CN.

The great extent of the hydrogen halo is illustrated by the Lyman-alpha isophotes of Comet Bennett (Fig. 4). From such isophotes, the number density of hydrogen atoms can be derived; the total area corresponds to some 10^{12} grams of hydrogen, while the profile implies the emission of approximately 10^{29} molecules of water per second per steradian. This result is consistent with

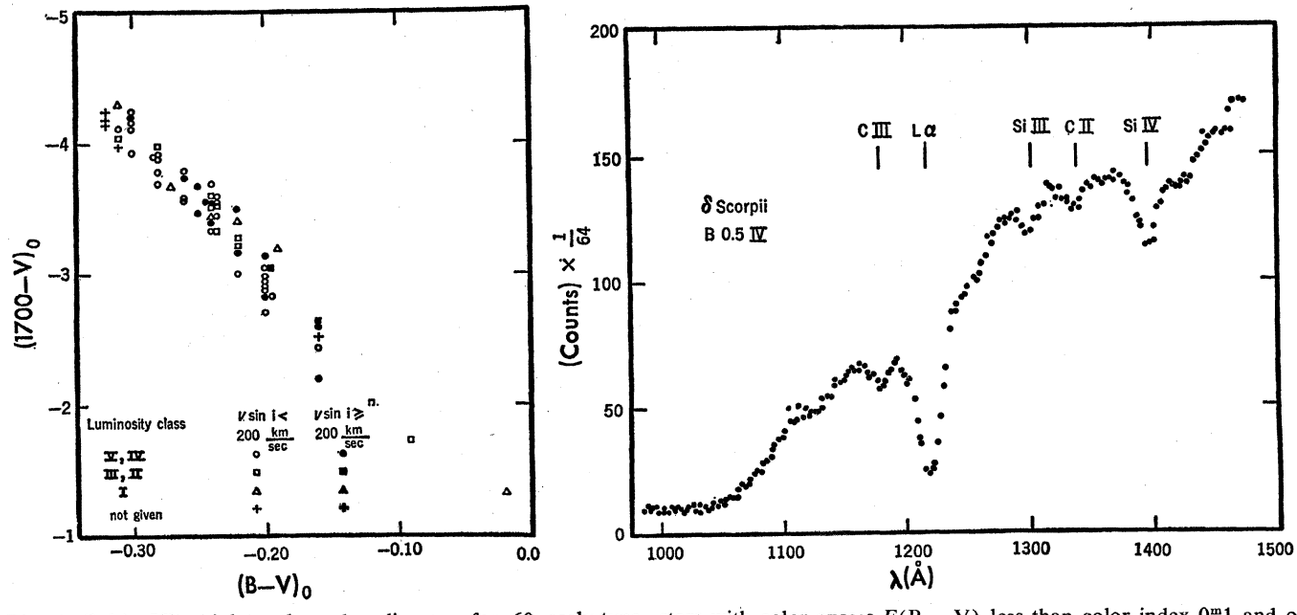

Fig. 1 (left). Ultraviolet color-color diagram for 60 early-type stars with color excess $E(B-V)$ less than color index 0^m1 and of a variety of spectral types, luminosity classes, and rotational velocities. The rotational velocity is v; the angle of inclination of a star's axis is i. The ordinate gives the difference in magnitude at 1700 Å and in the visual on a preliminary absolute scale; the abscissa is the standard B — V color determined from ground-based measurements. The B and V photoelectric magnitudes are measures of spectral regions with central wavelengths at 4200 and 5400 Å, respectively. The subscript zero denotes reduction to normal colors by means of extinction measurements. The magnitude at 1700 Å was obtained from spectrometer scans. [Adapted from (*18*); © 1972 by the University of Chicago] Fig. 2 (right). Scans of the star δ Scorpii (B0.5 IV, visual magnitude 2.33) over the region 1050 to 1430 Å. Raw counts are plotted against wavelength (λ). This composite scan was produced from four independent scans. Note the lines due to C III (1175 Å), Lyman alpha (Lα) (1216 Å), Si III (1300 Å), C II (1335 Å), and Si IV (1400 Å).

the measured isophotes of OH and suggests a lifetime for the OH radical of the order of 2×10^5 seconds. The hydrogen halo is found to be optically thick out to distances of the order of 10^5 kilometers. The line width is approximately 10 percent of the solar Lyman-alpha line width, and the observed surface brightness in the central 10 minutes of arc is essentially the same as the calculated reflected sunlight over this line width.

Another source of valuable information on the nature of cometary structure is provided by the variation of surface brightness with heliocentric distance. In both H and OH the brightness displays the same dependence on distance, varying approximately as the inverse sixth power. Delsemme (*8*) interprets this result as implying a three-step process for the H and OH halos, with each step involving approximately an inverse square dependence. Since virtually all the water would be dissociated within the halo the inverse square dependence of dissociation should not affect the observed surface brightness. The interpretation of these observations is therefore probably more complex than that described by Delsemme.

In the case of Comet Tago-Sato-Kosaka, observations were carried out through perigee. Thus, it was possible to measure the width of the comet's Lyman-alpha emission line by following the effects of the narrow absorption line due to the earth's geocorona as it moved across the comet's line with the changing Doppler shift. If the Lyman-alpha emission profile of the comet is Gaussian, then the Doppler width corresponds to a temperature of 1600°K.

Comet Tago-Sato-Kosaka was observed during the time in which its coma occulted the star π Piscium and Comet Bennett when it occulted σ Cassiopeiae. A preliminary analysis of these data indicates absorption of starlight in the center of the OH band for Comet Tago-Sato-Kosaka.

Ultraviolet Observations of the Planets

Planetary observations by OAO-2 are being analyzed by a group of guest investigators and Wisconsin astronomers. The satellite has obtained ultraviolet data on Venus, Mars, Jupiter, Saturn, Uranus, and Neptune. For Venus, Mars, Jupiter, and Saturn the data consist of spectral scans (resolution about 20 Å) over the region 2000 to 3000 Å and photometry at bands centered at 1500, 2000, 2500, 3000, 3300, and 4200 Å. In the case of the faint planets, Uranus and Neptune, the data consist of photometry at 2500, 3000, 3300, and 4200 Å. No planets have been detected with the short-wavelength spectrometer in the region 1050 to 1900 Å. Ultraviolet planetary observations are important because at the shorter wavelengths the effects of molecular scattering become more important than those of scattering from cloud particles or planetary surfaces. In addition, since many molecules and atoms have resonance lines in the ultraviolet, the presence or absence of a large number of interesting molecules can be more precisely established.

Determining the albedo or reflectivity as a function of wavelength is basic to the study of planetary atmospheres. For this purpose we need accurate solar spectral energy distributions. Although a number of ultraviolet observations of the sun have been made, most of these data are unsuitable for use in determining accurate ultraviolet planetary albedos (*9*). In the case of ground-based observations of the planets in the near ultraviolet, this difficulty has been overcome by comparing planetary spectra with observations of stars like our sun made with the same instrument. This method has the advantage that one does not need to know the instrumental sensitivity curve. The OAO has obtained good scanning results for such stars for wavelengths longer than about 2700 Å.

Figure 5 shows a new OAO ultraviolet albedo curve for Jupiter reported by Wallace *et al.* (*10*). Also shown in the figure are data obtained with ground-based instruments by Hopkins and Irvine (*11*) and Younkin and Munch (*12*). Their results agree well with the OAO data in the region of overlap. The albedo curve for Jupiter has a rise at shorter wavelengths that is probably due to Rayleigh scattering from molecular hydrogen. At about

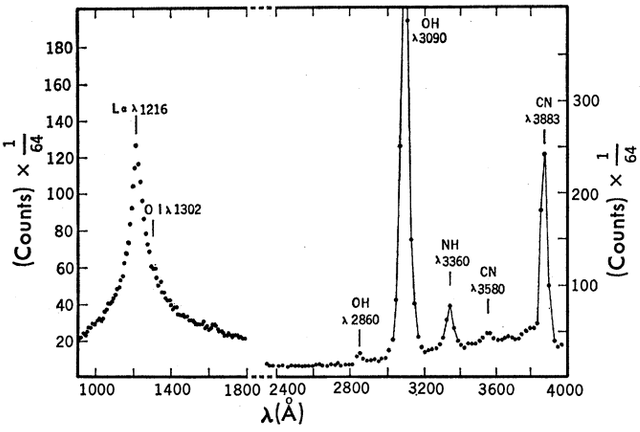

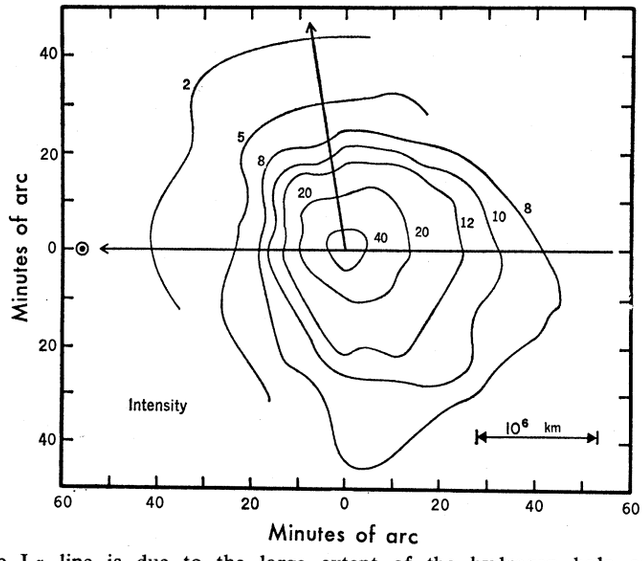

Fig. 3 (left). Ultraviolet spectrum of Comet Bennett (1969i). Raw counts are plotted against wavelength (λ). Some identified spectral lines or bands are due to Lyman alpha (Lα) (1216 Å), O I (1302 Å), OH (2860 and 3090 Å), NH (3360 Å), and CN (3580 and 3883 Å). Note how much stronger the OH band (3090 Å) is than the CN band (3883 Å). The great width of the Lα line is due to the large extent of the hydrogen halo as viewed by an objective-grating spectrometer (see Fig. 4). Fig. 4 (right). Hydrogen Lyman-alpha isophotes of Comet Bennett for 16 April 1970. The intensity units are kilo-Rayleighs. The full diameter of the halo at half intensity at the time of observation was approximately 20 minutes of arc, or about 7×10^5 kilometers.

2300 Å or less the albedo drops rapidly, indicating an increase in absorption which is most likely due to gaseous ammonia. The explanation of this albedo curve will undoubtedly involve scattering from both molecules and cloud particles. The actual albedo will depend in a complicated way on the nature of the cloud particles and their spatial distribution relative to the gaseous constituents of the atmosphere. A model to explain this albedo curve and other Jupiter data has been proposed by Axel (*13*).

It has been possible to search carefully for new narrow absorption features in the OAO planetary data by intercomparing spectral scans of one planet with those of another (*10*). In the case of the planets Mars, Jupiter, and Saturn no new narrow absorptions have been found. An upper limit of about 3 Å can be set for the equivalent width in the region 2100 to 3200 Å. These upper limits have been used to derive upper limits for the abundances of a large number of possible molecular constituents in the atmospheres of Saturn, Mars, and Jupiter (*14*).

The preliminary albedo curves discussed by Wallace (*15*) indicated that an average column density of 2×10^{-4} centimeter atmosphere of O_3 may be present in the atmosphere of Mars. However, those curves were based on an uncertain solar spectrum. Caldwell (*16*) has shown that the broad feature identified as O_3 by Wallace (*15*) was likely introduced by uncertainties in the solar spectrum. A detailed analysis of Mars' albedo curve was made by Caldwell (*17*). He concluded that the albedo could be matched by invoking Rayleigh scattering from the known amount of atmospheric CO_2 (80-meter atmospheres) and a slowly decreasing ground albedo toward shorter wavelengths. The derived ground albedo disagrees with reflectivities expected for a number of suggested ground materials.

OAO Observations of Interstellar Dust

The OAO can provide valuable new information on the scattering characteristics of the interstellar dust. Observations of diffuse galactic light can be used to obtain information on the ultraviolet albedo and phase function of the dust, while observations of reddened stars can be used to derive its extinction characteristics. Here we discuss the OAO extinction data. Of

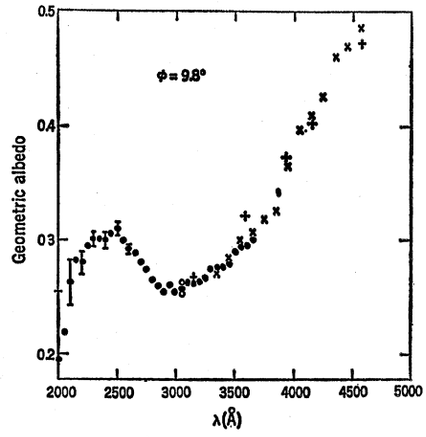

Fig. 5. Ultraviolet albedo of Jupiter for the phase angle (ϕ) of 9.8°. The OAO curves (open and closed circles) were obtained from data for G-type stars for wavelengths (λ) above 2700 Å and from a new photoelectric solar spectrum of Broadfoot (*40*) for wavelengths below 2700 Å. (Closed circles) OAO spectrometer data; (open circles) OAO broadband photometry data; (+) data from ground-based observations by Hopkins and Irvine (*11*); (×) data from ground-based observations by Younkin and Munch (*12*). [Adapted from (*10*); © 1972 by the University of Chicago]

the approximately 300 O-type and B-type stars observed by OAO-2 up to February 1972, about 75 are suitable for deriving interstellar extinction curves.

Figure 6 shows four extinction curves derived from scanner data (*18*). The curves were obtained by intercomparing reddened and unreddened stars of the same spectral type and, when possible, the same luminosity class. The general characteristics of these curves are: (i) a pronounced bump, which in most cases peaks at 2175 ± 25 Å (in Fig. 6, the reciprocal wavelength equals 4.6 reciprocal micrometers); (ii) a broad minimum somewhere in the region 1800 to 1300 Å (reciprocal wavelength between 5.5 and 7.5 μm^{-1} in Fig. 6); (iii) a rapid rise in extinction toward the far ultraviolet; and (iv) significant variations in ultraviolet extinction, the variations being greatest in the far ultraviolet.

Although a satisfactory detailed interpretation of the OAO extinction curves does not yet exist, many theoretical suggestions have emerged. For example, Stecher (*19*), Gilra (*20*), and Wickramasinghe and Nandy (*21*) believe that graphite particles may be responsible for the pronounced bumps; Huffman and Stapp (*22*) attribute them to silicates; Manning (*23*) suggested quartz; and Graham and Duley (*24*) indicated that solid hydrocarbons could produce the bumps. A review of all these suggestions and a discussion of the physics of extinction bumps has been given by Gilra (*25*), who concludes that the most likely cause of the bumps is plasma oscillations in small (mean radius about 100 Å), uncoated, interstellar graphite particles.

The observed variation in shape of the extinction curves demonstrates that multicomponent models of interstellar particles are probably required. In Fig. 6 one can see that the bumps for ξ Persei, β^1 Scorpii, and σ Scorpii are similar, but the far-ultraviolet extinction is quite different for each star. Thus, the material responsible for the far-ultraviolet extinction is probably different from that producing the extinction at the bump.

The OAO observations of diffuse galactic light are being studied by Witt and Lillie (*26*). The studies of diffuse light and reflection nebulas together with the extinction data should provide a better understanding of the nature of interstellar particles and are helpful in understanding ultraviolet radiation from extragalactic systems.

Interstellar Lyman-Alpha Absorption

The short-wavelength spectrometer on board OAO-2 has a spectral resolution adequate for making measurements of the strong Lyman-alpha absorption line at 1216 Å due to interstellar neutral hydrogen. This line has been observed in approximately 70 stars of spectral type B2 or earlier. For stars later than B2 the stellar Lyman-alpha line is very strong, making useful measurements of interstellar absorption difficult. Although radio astronomers have obtained an enormous amount of information on the distribution and kinematics of the neutral hydrogen from studies of the 21-centimeter line, the new Lyman-alpha absorption data are unique because they make it possible to investigate the relationship between the amounts of interstellar hydrogen and other interstellar constituents, such as atoms, molecules, and grains, along precisely the same path. Radio observations of 21-cm emission usually average the brightness distribution over a large solid angle (usually about 1° in diameter), and the path length over which the emission occurs is often uncertain. Optical measurements of gas and dust and Lyman-alpha measurements subtend an infinitesimal sampling

area (the projected area of the star). The uncertainty in the path length for the radio data was revealed when the first Lyman-alpha absorption data were obtained in the rocket experiments of Morton (*27*). These early observations yielded the unexpected result that the column density of hydrogen in the directions of δ Orionis and ζ Orionis was about 1.5×10^{20} atoms per square centimeter, corresponding to an average space density of 0.1 atom per cubic centimeter, instead of the 1.3×10^{21} cm^{-2} or 1 cm^{-3} derived from 21-cm emission data.

A preliminary analysis of the OAO Lyman-alpha data, reported by Savage and Code (*28*), revealed that the spectral resolution was not adequate to separate the interstellar Lyman alpha from neighboring stellar absorption lines. Because of this line blending, upper limits to the hydrogen column density as obtained from the OAO data were presented, and important conclusions were drawn from them. Since that report researchers from Wisconsin and Princeton universities have attempted to account for the effects of stellar line blending and to resolve disagreements between the rocket data and the OAO data. In a number of cases the OAO upper limits were significantly larger (two to three times) than published rocket results. Most of these differences have since been attributed to a number of factors that involve both OAO and rocket data, such as line blending, placement of the continuum levels, and incorrect allowance for the broad wings of the Lyman-alpha line.

Savage and Jenkins (*29*) have shown that it is possible to make reasonably accurate determinations of the hydrogen column density from OAO data for about 70 stars. These measurements were made by using the higher-resolution rocket data as a guide in determining the amount of line blending in the OAO data. Figure 7 shows some composite line profiles made from the OAO data in the region of the Lyman-alpha line. The small amount of scatter in the data is usually equal to that introduced by photon statistics. The dip shortward of Lyman alpha is due to a multiplet of C III at 1175 Å. Contained in the line centered at 1216 Å is a line due to Si III at 1206 Å, which mainly contributes to the line blending for stars of spectral types later than B0. For earlier stars a doublet of N V at about 1240 Å begins to contribute to the line blending. In Fig. 7 one can see the increase in strength of the Lyman-alpha line with the B − V color excess of the star. In the case of the star δ Scorpii the OAO line profile is compared with a recent observation of the Princeton rocket group (*30*). The higher-resolution Princeton data has been smoothed to the OAO resolution. Except for a slight difference between the stellar lines on the long-wavelength wing of Lyman alpha, probably due to residual absorption in the rocket measurements, the agreement is excellent for data obtained by two totally different methods.

When OAO Lyman-alpha column densities were compared with those obtained from 21-cm emission measurements, very poor correlation was found (*29*). In contrast, the OAO column densities correlate well with Na I and Ca II column densities and with the $E(B - V)$ measurements. These new data were used to determine the abundance ratios of sodium and calcium to hydrogen as well as the ratio of mass densities of hydrogen to dust in the interstellar medium. The results obtained were 2.3×10^{-7} for Na/H, 6.8×10^{-9} for Ca/H, and approximately 100 for ρ_H / ρ_d.

The average space density of hydrogen for all the Lyman-alpha stars observed was 0.6 cm^{-3}. For these stars the average distance from the earth was 300 parsecs. If one only uses stars with distances less than 140 parsecs an average hydrogen space density of 0.25 cm^{-3} is obtained. In

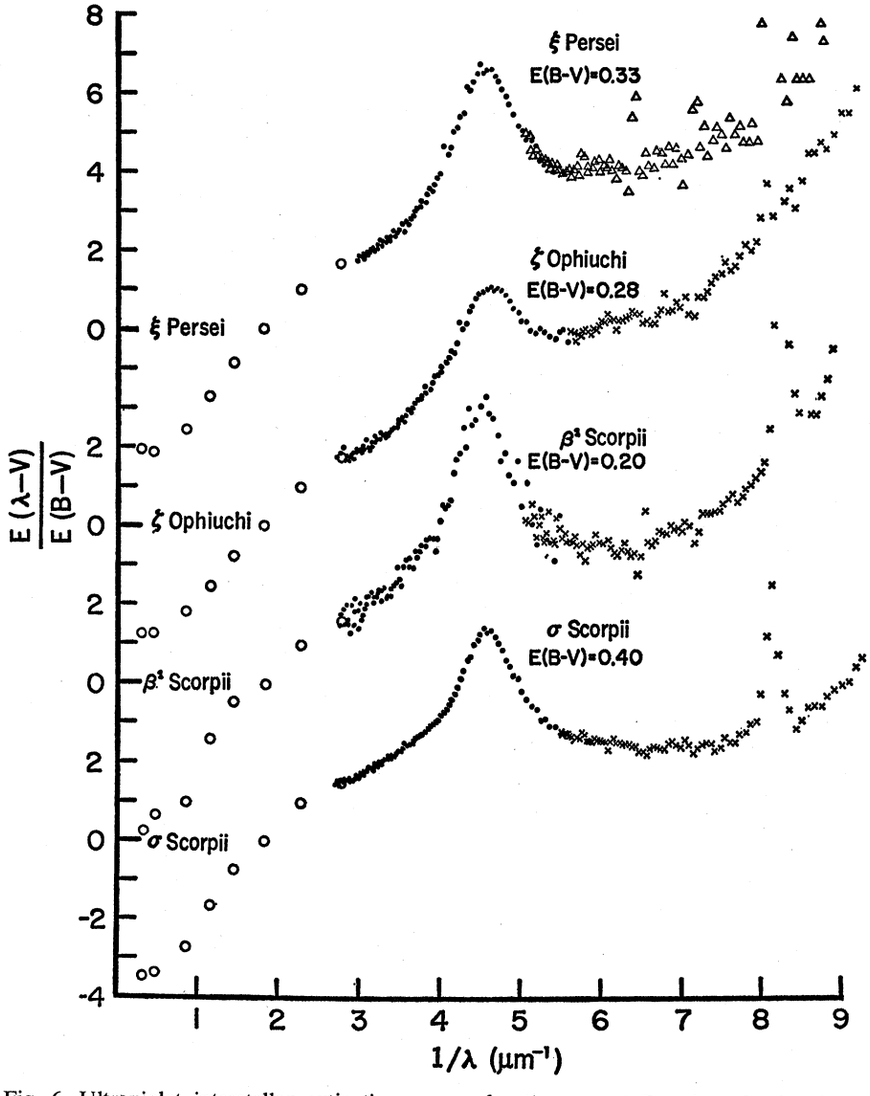

Fig. 6. Ultraviolet interstellar extinction curves for the stars ξ Persei, ζ Ophiuchi, β^1 Scorpii, and σ Scorpii; $E(\lambda - V)$, extinction in magnitudes or color excess between a wavelength λ and the photoelectric visual band; $E(B - V)$, the B − V color excess. These curves show magnitudes of extinction normalized to an $E(B - V)$ color excess of 1^m0 plotted as a function of reciprocal wavelength in reciprocal micrometers. Note the large differences in ultraviolet extinction between these stars. [Adapted from (*18*); © 1972 by the University of Chicago]

contrast to the early rocket results, which included only a few stars, the average space density of hydrogen obtained from the OAO Lyman-alpha data does not differ greatly from average space densities derived from 21-cm radio data.

Ultraviolet Emission Lines

Ultraviolet emission lines are of great interest for the clues they provide to the structure of extended, often violently moving, stellar atmospheres. Morton (*27*) discovered that a few early-type stars in Orion are surrounded by rapidly expanding shells. Evidence for these expanding shells came from ultraviolet spectra obtained from rockets, which showed emission line profiles of the P-Cygni type for the strong ultraviolet resonance doublets of Si IV (1394 and 1403 Å) and C IV (1548 and 1551 Å). Typical velocities were in the range 1000 to 2000 kilometers per second. Such large velocities suggest that the rate of mass loss by these early-type supergiants might significantly influence the evolution of the star. Furthermore, high rates of mass loss may significantly disturb the surrounding interstellar medium.

The OAO has been used to supplement the early rocket results with observations of a larger number of stars (Table 1 and Fig. 8). Even at the relatively low spectral resolution of OAO-2 one can see P-Cygni profiles in certain early-type stars. Examples are the Si IV and C IV doublets in the spectrum of γ Velorum (WC 7), shown in Fig. 8. Because of the high quality of the OAO data, good determinations can be made of the equivalent widths of these strong ultraviolet lines (*31*). Finally, since the extended lifetime of OAO-2 has made possible a survey of most of the early-type stars brighter than 5 in visual magnitude, it should now be possible to determine in what parts of the Hertzsprung-Russell diagram the mass-loss phase occurs.

A number of peculiar stars exhibiting emission lines have been observed. For example, β Lyrae (see Fig. 8 and Table 1) is an eclipsing binary system, one component of which is a hot B-type star. Mass exchange occurs between the two stars, and this gas in the intense radiation field produces a large number of emission lines. The OAO has obtained spectral scans and photometry data for β Lyrae throughout its 13-day cycle, and these data have been released to interested astronomers through the data bank of the National Aeronautics and Space Administration. An interpretation of these data is given by Kondo, McCluskey, and Houck (*32*), who speculate that one of the components may be a gravitationally collapsed star or a black hole.

Many observations have been made of cool, late-type stars, the data consisting of both spectral scans (for the brightest of these stars) and photometry. The value of such observations for determining ultraviolet planetary albedos has been discussed above, and we are concerned here with ultraviolet emission lines observed in late-type stars. An analysis of the spectral scans by Doherty (*33*) has shown emission in the Mg II doublet (2796 and 2803 Å) in a number of late-type giants and supergiants. Figure 8 shows the OAO ultraviolet scans of α Boötis (K2 IIIp) and α Orionis (M2 Iab). In these spectra Mg II is seen in emission above the adjacent continuum level. A list of late-type stars definitely showing Mg II emission at the OAO resolution appears in Table 1.

Like the H and K emission lines of Ca II, the Mg II emission lines in cool stars provide information on the structure of stellar chromospheres. Details of the Mg II profiles cannot be obtained with OAO resolution. However, Doherty (*34*) finds that the relative strength of the Mg II and Ca II emissions for eight giants and supergiants is nearly constant and about equal to the relative strength observed in the sun. This result is difficult to understand because one would expect the relative strength of these emission lines to be very sensitive to physical conditions in the chromospheric regions of stars. A possible but unlikely interpretation of this observation is that the regions of the atmospheres that form Ca II and Mg II emission may be quite similar in all late-type stars. Further theoretical work is needed to fully explore the implications of this result.

Although a search has been made for emission lines other than those of Mg II in late-type stars, none has been definitely detected. However, it is likely that an instrument with higher resolution, such as the spectrometer in the next orbiting observatory (OAO-C), will reveal other chromospheric lines, as well as weak emission in the bottom of the Mg II absorption line, in most late-type stars.

The OAO-2 spectrometers and photometers have observed a number of diffuse and planetary nebulas. Unfortunately, no emission lines have yet been unambiguously detected in these objects. It appears that more sensitive instrumentation will be required for observa-

Table 1. Sample listing of some of the ultraviolet emission lines so far observed by OAO-2. Included in the table are emission lines detected in early-type stars, late-type stars, peculiar stars, a nova, and comets; m_v, visual magnitude.

Object	Spectral type	m_v	Ultraviolet emission lines (Å)
HD 50896	WN5	6.90	N V (1230, 1243), N IV (1496), C IV (1548, 1551), He II (1640), N IV (1718), He II (2740), He II (3203), N IV (3480)*
γ Velorum	WC7	1.82	Si IV (1394, 1403), C IV (1548, 1551), He II (1640), N V (1719), C III (1909), C IV (1923), C III (2298), C IV (2405), C IV (2525)
ζ Puppis	O5 f	2.25	N V (1239, 1243), C IV (1548, 1551), He II (1640), N IV (1719)
ζ Orionis	O9.5 Ib	1.73	Si IV (1394, 1403), C IV (1548, 1551)
α Camelopardalis	O9.5 Ia	4.30	Si IV (1394, 1403)
κ Orionis	B0.5 Ie	2.06	Si IV (1394, 1403), C IV (1548, 1551)
β Lyrae	B9 pc	3.40	Lα (1216), Si IV (1394, 1403), C IV (1548, 1551), Mg II (2796, 2803)*
α Boötis	K2 IIIp	0.06	Mg II (2796, 2803)
ϵ Pegasi	K2 Ib	2.40	Mg II (2796, 2803)
α Tauri	K5 III	0.86	Mg II (2796, 2803)
β Andromedae	M0 III	2.03	Mg II (2796, 2803)
α Scorpii	M1 Ib	1.08	Mg II (2796, 2803)
α Orionis	M2 Iab	0.86	Mg II (2796, 2803)
Nova Serpentis 1970			Mg II (2796, 2803)*
Comets 1969g and 1969i			Lα (1216), O I (1302), OH (2860), OH (3090), NH (3360), CN (3580), C_3 (3680), CN (3883), C_2 (4000)*

* Plus unidentified lines.

tions of ultraviolet emission lines in gaseous nebulas. It is possible, however, to study the continuous spectra of nebulas. Holm (*35*), for example, has interpreted the continuous ultraviolet spectra of planetary nebulas in terms of Balmer and two-photon emission by atomic hydrogen.

Ultraviolet Observations of Nova Serpentis 1970

Observations of Nova Serpentis 1970 were obtained throughout the first 60 days after its outburst in February 1970 with both the filter photometers and the long-wavelength spectrometer (*36*). Over this period, the spectrum evolved from an absorption line spectrum similar to that of a reddened F star to a strong emission line spectrum. At the spectral resolution of 20 Å, the emission lines first made their appearance about 6 days after discovery. The change in the appearance of the spectra in the region from 2500 to 3500 Å is illustrated in Fig. 9. While the light was steadily dropping in the visual and photographic, both the underlying continuum and the broad emission features continued to brighten. The visual brightness decreased about 2.5 magnitudes, while the flux in the region of the Mg II resonance lines increased by about 1.5 magnitudes. If we attribute this increase of line strength through the first 50 days to an optically thick shell and assume that the optical depth becomes unity where the strength begins to decrease, we may estimate the total number of Mg II ions. The result is consistent with the usual estimates of mass loss by a nova.

The energy distribution defined by the filter photometry data and data from ground-based observations yields approximately constant total flux in the interval from 1000 to 6000 Å during the first 60 days, the decrease in light in the visual being due to a shift of the energy curve toward the ultraviolet as the system evolves. These results suggest a model in which the bolometric luminosity remains relatively constant, but the conversion of far-ultraviolet photons to longer wavelengths undergoes a secular change as the density of the shell decreases. The system is thus somewhat analogous to the rapid evolution of a planetary nebula.

The ultraviolet energy curve as well as B − V color measurements suggest an interstellar visual extinction of the order of two magnitudes. If this extinction is produced by a nearby dust cloud, the energy absorbed by the grains is sufficient to account for the infrared emission commencing about 50 days after outburst and reaching a maximum at about 90 days. However, other models for the infrared flux are also suggested by the observations described here.

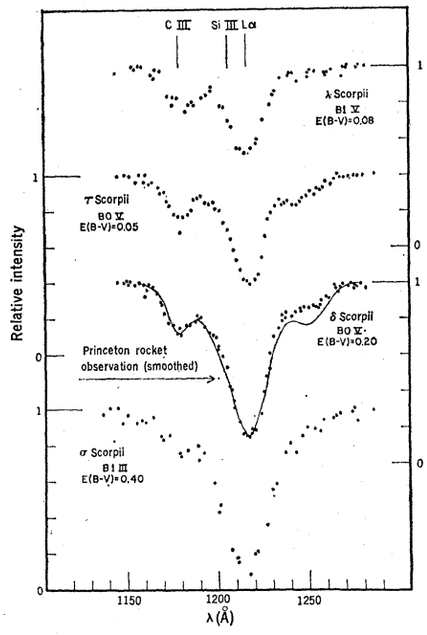

Fig. 7. Lyman-alpha line profiles obtained by OAO-2 for four stars in the Scorpius region. These are composite line profiles obtained by combining a number of independent scans made with the normal stepping interval (10 Å between data points) of the short-wavelength spectrometer. Contained in the strong line at 1216 Å are contributions from stellar lines and from the interstellar Lyman-alpha (Lα) line. The solid line drawn through the data for δ Scorpii is an observation of the Princeton rocket group (*30*) smoothed to the OAO resolution. Note that the stars with the largest amount of interstellar reddening (δ Scorpii and σ Scorpii) have the strongest Lyman-alpha lines). The B − V color excesses are listed in the figure.

Ultraviolet Photometry of Galaxies

To date, OAO observations have been reduced for 35 galaxies of diverse morphological types (*37*). The measurements were made with the filter photometers and a 10-arc-minute diaphragm.

In Fig. 10 the ultraviolet emissions of galaxies and main-sequence stars are compared. Galaxies are systematically brighter shortward of 2500 Å than stars of similar spectral distribution in the photographic and visual region of the spectrum. For the same B − V colors, the galaxies are approximately three magnitudes bluer than main-sequence stars at 1920 Å. Late-type giant stars fall about midway between the galaxies and main-sequence stars. Two Seyfert galaxies, NGC 4051 and NGC 1068, are included in Fig. 10. Their colors do not deviate from those of normal galaxies.

Figure 11 shows the spectral energy curves for the spiral galaxy M 94 (Sb) and the elliptical galaxy M 102 (E6p). These curves are based on a preliminary absolute calibration of the photometers and give the approximate flux per unit wavelength interval relative to the wavelength $\lambda = 3330$ Å. These curves are typical of the results for most spiral and elliptical galaxies, although the curves for the latter are poorly determined shortward of 2400 Å. The spectral distributions of spiral galaxies are understandable in terms of the contribution from early-type stars (presumably in the spiral arms), modified by interstellar absorption. The results for elliptical galaxies, in which the energy distribution appears to rise steeply shortward of 2500 Å, cannot be interpreted in terms of early-type stars alone. The energy distribution for an infinite-temperature blackbody would rise with a slope of λ^{-4} while these curves rise as steeply as λ^{-20}. It is difficult to

Table 2. Sample list of variable stars observed by OAO-2.

Star	Spectral type	Comments		Period (days)
		Variable	Type	
β Lyrae	B5 p + ?	Eclipsing	β Lyrae	12.9
VV Orionis	B2 + B8	Eclipsing	β Lyrae	1.48
CW Cephei	B1.5 + B1.5	Eclipsing		2.73
U Ophiuchi	B5 + B5	Eclipsing	Algol	1.68
RR Lyrae	A8	Pulsating	RR Lyrae	0.57
β Doradus	F8 Ia	Pulsating	Cepheid	9.84
β Canis Majoris	B1 II	Pulsating	β Canis Majoris	0.25
β Cephei	B1 II	Pulsating	β Canis Majoris	0.19
α^2 Canum Venaticorum	B9.5 p	Magnetic, spectrum		5.47

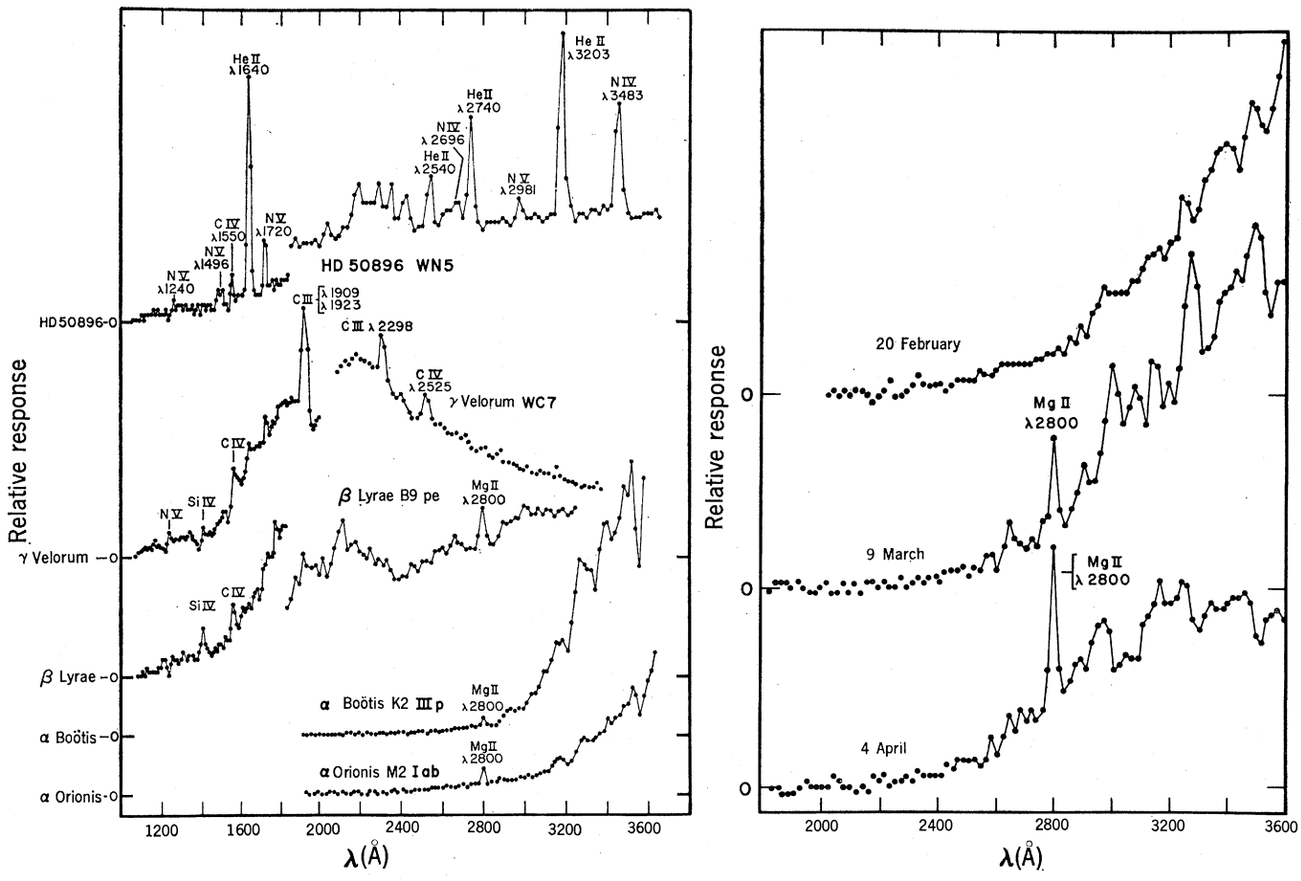

Fig. 8 (left). Spectra of five stars showing ultraviolet emission lines. Relative response is plotted against wavelength (λ). No attempt has been made to properly join data from the short-wavelength spectrometer onto data from the long-wavelength spectrometer. The response scale has been arbitrarily adjusted for each of the objects by a constant scale factor so that all emission lines could be seen in one diagram. Some of the identified emission lines are labeled. See Table 1 for a more complete listing of emission line objects. Fig. 9 (right). Ultraviolet spectra of Nova Serpentis 1970 for 20 February, 9 March, and 4 April 1970. Note the changing appearance of the continuum and the Mg II doublet (2800 Å) as the nova evolves.

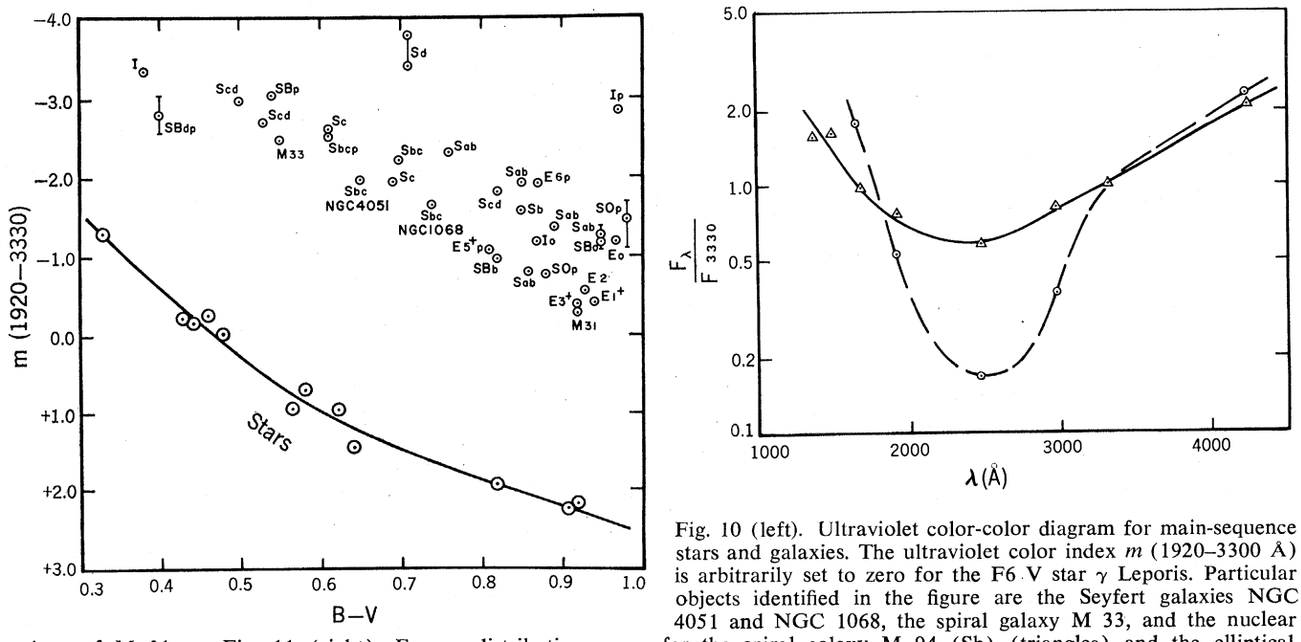

Fig. 10 (left). Ultraviolet color-color diagram for main-sequence stars and galaxies. The ultraviolet color index m (1920–3300 Å) is arbitrarily set to zero for the F6 V star γ Leporis. Particular objects identified in the figure are the Seyfert galaxies NGC 4051 and NGC 1068, the spiral galaxy M 33, and the nuclear regions of M 31. Fig. 11 (right). Energy distribution curve for the spiral galaxy M 94 (Sb) (triangles) and the elliptical galaxy M 102 (E6p) (circles). These curves are based on a preliminary absolute calibration. The flux (F) per unit wavelength interval is given relative to the wavelength $\lambda = 3330$ Å.

imagine any reasonable source, thermal or nonthermal, that would behave in this manner. It may be significant that the minimum of these curves is near the maximum of our interstellar extinction curve. If it is assumed that elliptical galaxies do contain significant quantities of dust and that the albedos of the particles decrease in the vicinity of the 2200-Å interstellar extinction peak, it is possible to reproduce the observed curves. It would then also be true that a significant fraction of the bolometric luminosity of the galaxy is radiated by these grains in the infrared.

These OAO observations should prove important for furthering our understanding of many problems of extragalactic astronomy, including the stellar luminosity function, interstellar absorption in galaxies, K-term corrections required in photometry of distant, redshifted galaxies, and the magnitude of brightness of the extragalactic sky.

Variable Stars

Extensive ultraviolet observations have been obtained for variable stars of diverse types (a small sample list is given in Table 2). Figure 12 shows some typical ultraviolet light curves obtained by Molnar (*38*) for the magnetic variable α^2 Canum Venaticorum. In the visible part of the spectrum this unusual star exhibits spectral variations of line intensities and radial velocities of overabundant rare-earth and iron-peak elements. Furthermore, with the same period there is a strong magnetic field variation from −4000 to +5000 gauss. The most common interpretation of these variations is that a magnetic dipole field is inclined to the axis of rotation of the star, and concentrations or patches overabundant in certain elements rotate with the star, producing spectral changes. The OAO light curves for this star indicate that at the maximum intensity of the rare-earth lines, the ultraviolet continuum shortward of 2900 Å is greatly diminished while the visual spectral region becomes brighter. Molnar (*38*) has interpreted this as being due to the variable strong line-blanketing by the abundant rare-earth elements. The small scatter in the data of Fig. 12 illustrates the quality of OAO-2 photometry in cases for which the observations are carefully made and reduced.

There are three important features of these measurements of variable stars. First, these observations extend

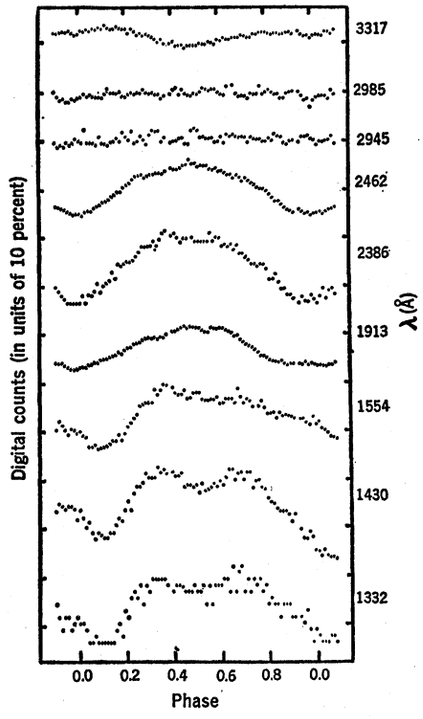

Fig. 12. Ultraviolet light curves for the magnetic spectrum variable α^2 Canum Venaticorum from Molnar (*38*). The numbers to the right of the figure are photometer filter wavelengths. The digital counts are relative to phase 0.0.

investigations to a previously unexplored spectral region. Thus, new phenomena are observed and new insights gained. Examples are the variations of Lyman alpha in β Lyrae reported by Houck (*39*) and their interpretation in terms of gas flow in the system. Second, these observations supplement the classical treatment of variable stars by extending the spectral region covered and by the fact that they are often of higher accuracy than ground-based photometry. Finally, since complete coverage in time is possible from an orbiting observatory, complete light curves are obtained over a single period with the same instrument for stars for which this could not be accomplished from the ground.

Summary

In this article scientific results obtained by the Wisconsin experiment package on board OAO-2 have been reviewed. Included in the review are results of ultraviolet observations of stars, comets, planets, interstellar dust, interstellar hydrogen, objects with ultraviolet emission lines, Nova Serpentis 1970, galaxies, and variable stars.

References and Notes

1. A. L. Hammond, *Science* **170**, 960 (1970); A. D. Code, *Publ. Astron. Soc. Pac.* **81**, 475 (1969); ———, T. E. Houck, J. F. McNall, R. C. Bless, C. F. Lillie, *Sky Telesc.* **38**, 290 (1969); A. D. Code, *Space Research XI* (Akademie-Verlag, Berlin, 1971), p. 1339.
2. The ultraviolet star catalog of the Smithsonian Astrophysical Observatory and discussions based on these data, as well as results obtained by other investigators, can be found in the proceedings of the symposium on OAO-2 held in Amherst, Massachusetts, on 22 and 23 August 1971 [*Proceedings of the OAO Symposium* (NASA-SP 310, National Aeronautics and Space Administration, Washington, D.C., in press)].
3. A. D. Code, T. E. Houck, J. F. McNall, R. C. Bless, C. F. Lillie, *Astrophys. J.* **161**, 377 (1970).
4. A. D. Code, T. E. Houck, C. F. Lillie, *IAU Announcement Card 2201* (1969); T. E. Houck and A. D. Code, *Bull. Amer. Astron. Soc.* **2**, 321 (1970); A. D. Code, T. E. Houck, C. F. Lillie, in *Proceedings of the OAO Symposium* (NASA-SP 310, National Aeronautics and Space Administration, Washington, D.C., in press).
5. L. Biermann and E. Trefftz, *Z. Astrophys.* **59**, 1 (1964).
6. E. B. Jenkins and D. W. Wingert, *Astrophys. J.* **174**, 697 (1972).
7. J. L. Bertaux and J. Blamont, *C. R. H. Acad. Sci. Ser. B* **270**, 1581 (1970).
8. A. H. Delsemme, *Science* **172**, 1126 (1971).
9. R. C. Anderson, J. G. Dipes, A. L. Broadfoot, L. Wallace, *J. Atmos. Sci.* **26**, 874 (1969).
10. L. Wallace, J. Caldwell, B. D. Savage, *Astrophys. J.* **172**, 755 (1972).
11. N. B. Hopkins and W. Irvine, in *Proceedings of IAU Symposium No. 40*, C. Sagan, Ed. (Springer-Verlag, New York, 1971), p. 349.
12. R. L. Younkin and G. Munch, *Mem. Soc. Roy Sci. Liège Ser. 5* **7**, 125 (1963).
13. L. Axel, "Inhomogeneous Models of the Atmosphere of Jupiter," preprint.
14. C. Sagan and T. Owen, in *Proceedings of the OAO Symposium* (NASA-SP 310, National Aeronautics and Space Administration, Washington, D.C., in press).
15. L. Wallace, *Bull. Amer. Astron. Soc.* **2**, 240 (1970).
16. J. Caldwell, thesis, University of Wisconsin (1970).
17. ———, *Icarus*, in press.
18. R. C. Bless and B. D. Savage, *Astrophys. J.* **171**, 293 (1972).
19. T. P. Stecher, *Astrophys. J. Lett.* **157**, 125 (1969).
20. D. P. Gilra, *Nature* **229**, 237 (1971).
21. N. C. Wickramasinghe and K. Nandy, *ibid.*, p. 81.
22. D. R. Huffman and J. L. Stapp, *ibid.*, p. 45.
23. P. G. Manning, *ibid.*, p. 115.
24. W. R. M. Graham and W. W. Duley, *ibid.* **232**, 43 (1971).
25. D. P. Gilra, in *Proceedings of the OAO Symposium* (NASA-SP 310, National Aeronautics and Space Administration, Washington, D.C., in press).
26. A. N. Witt and C. F. Lillie, in *ibid.*
27. D. C. Morton, *Astrophys. J.* **147**, 1017 (1967).
28. B. D. Savage and A. D. Code, in *Proceedings of IAU Symposium No. 36*, L. Houziax and H. E. Butler, Eds. (Springer-Verlag, New York, 1970), p. 302.
29. B. D. Savage and E. B. Jenkins, *Astrophys. J.* **172**, 491 (1972).
30. E. B. Jenkins, private communication.
31. A. D. Code and R. C. Bless, in *Proceedings of IAU Symposium No. 36*, L. Houziax and H. E. Butler, Eds. (Springer-Verlag, New York, 1970), p. 173.
32. Y. Kondo, G. McCluskey, T. Houck, *Proceedings of the OAO Symposium* (NASA-SP 310, National Aeronautics and Space Administration, Washington, D.C., in press).
33. L. Doherty, *Phil. Trans. Roy. Soc. London Ser. A* **270**, 189 (1971).
34. ———, in *Proceedings of the OAO Symposium* (NASA-SP 310, National Aeronautics and Space Administration, Washington, D.C., in press).
35. A. Holm, in *ibid.*
36. A. D. Code, in *ibid.*
37. ———, G. A. Welch, T. Page, in *ibid.*
38. M. R. Molnar, in *ibid.*
39. T. Houck, in *ibid.*
40. A. L. Broadfoot, *Astrophys. J.* **173**, 681 (1972).